fluids

MDPI

Article

The Influence of Mitral Valve Asymmetry for an Improved Choice of Valve Repair or Replacement

Dario Collia [1,*,†] and Gianni Pedrizzetti [1,2,†]

[1] Department of Engineering and Architecture, University of Trieste, 34127 Trieste, Italy
[2] Department of Biomedical Engineering, University of California, Irvine, CA 92617, USA
* Correspondence: dario.collia@dia.units.it
† These authors contributed equally to this work.

Abstract: The study of valve asymmetry represents an important avenue for modern cardiac surgery. The correct choice of leaflet reconstruction may indicate a new path in the quality and long-term survival of patients. A systematic investigation was performed with a total of 25 numerical simulations using a healthy ventricle and an ideal valve with varying degrees of valve asymmetry. An overall assessment is made in terms of vorticity, kinetic energy, dissipated energy, and hemodynamic forces. The results indicate that the optimal asymmetry to consider for a valve repair or prosthetic design is between 0.2 and 0.4 with an optimal point of about 0.3. Out of this range, the heart is subjected to an excessive workload, which can only worsen the patient's state of health.

Keywords: CFD; mitral valve; valvular asymmetry; cardiovascular flow

Citation: Collia, D.; Pedrizzetti, G. The Influence of Mitral Valve Asymmetry for an Improved Choice of Valve Repair or Replacement. *Fluids* **2022**, *7*, 293. https://doi.org/10.3390/fluids7090293

Academic Editor: Mehrdad Massoudi

Received: 12 August 2022
Accepted: 2 September 2022
Published: 5 September 2022

1. Introduction

The function of the mitral valve (MV) is to allow and regulate the correct access of blood into the left ventricle (LV). The MV has a characteristic elliptical shape and is composed of an annulus and two leaflets, posterior and anterior, respectively. Its function is crucial for correct ventricular functioning as it directs the flow within it, ensuring correct mixing and redirection of blood towards the aorta in healthy conditions. On the other hand, in pathological conditions, the leaflets of the MV have prolapsed and a quantity of the blood is regurgitated into the atrium during the systole. Depending on the different types of mitral regurgitation (MR) [1], there are different therapeutic solutions; in particular, in the cases of severe MR, the therapy is usually a cardiac surgery for valve repair or, less frequently, valve replacement with a prosthesis. Over the years, different methods have been developed to treat this pathology. The first option was the substitution with a mechanical or biological prosthetic valve; this, however, brings along several complications [2,3]. To date, the recommended treatment for degenerative mitral valve disease is mitral valve repair (MVR), as opposed to valve replacement with a biological or mechanical valve, because surgical valve reconstruction is associated with improved event-free survival [4,5]. Surgical MVR is the gold-standard therapeutic procedure for patients with degenerative mitral valve regurgitation [4,6] and follows two fundamental principles: restoring a good surface of leaflet coaptation and correcting for annular dilatation [4,7]. Transcatheter solutions represent additional options that are currently recommended only in patients at risk [5,8,9]. Although the reparation is the gold standard, endovascular replacement is expected to increase with the improvement in and availability of endovascular prostheses. One important point to consider during the planning of valve repair or for the good design of a valve prosthesis is the identification of the appropriate range of valve asymmetry [10]. The present study uses the approach of direct numerical simulation (DNS) to provide indication of this range. Several techniques have been introduced in the literature to overcome the numerical difficulties due to the movement of the numerical domain, including the formulations of space-time finite elements, immersed boundary methods, the method of level sets,

the fictitious domain method, unfit finite elements and the arbitrary Lagrangian–Eulerian formulation (ALE) [11–14]. The numerical method, used in this work, was extensively employed in previous studies, and technical details are described in a dedicated methodological validation study [15], where the valvular dynamics were compared with that obtained with complete fluid–structure interaction [16]. In a previous study [10], the proper range of valve asymmetry is investigated in terms of false and effective regurgitation, as well as a thorough distribution of washout in healthy, pathological, and repaired cases with different levels of valve asymmetry. Therein, the physiological degree of asymmetry was found to be associated with small regurgitation and a proper ventricular wash-out for normal ventricles. This work follows up to provide a more comprehensive assessment and indication of the proper range of valve asymmetry to be used for a repair or prostheses design, and we extend the previous study and analyze the results from an energetic and mechanical point of view by investigating how valve asymmetry affects hemodynamic forces and the amount of kinetics energy produced and dissipated.

2. Materials and Methods

2.1. Geometries

A total of 25 numerical simulations were performed and analyzed using the same healthy LV for 25 MVs, each with a different degree of valve asymmetry. The time-varying geometry of a healthy LV has been extracted from 3D echocardiography; the moving borders were obtained by a semi-automatic procedure within a dedicated software (4D LV analysis, Tomtec Imaging Systems GmbH, Unterschleissheim, Germany). At every instant, the entire LV endocardial surface is described by its 3D coordinates, which are then interpolated on a structured mesh made of 768 points along the circumference and 384 points from the base to the apex. LV geometry during all phases of the heartbeat is described by the position vector $\mathbf{X}(\vartheta, s, t)$ of its endocardial surface, where the structured parametric coordinates (ϑ, s) run along the circumference and from base to apex, respectively, and t is time. The position vector marks the material points of the LV, and their velocity is obtained from temporal differentiation. The LV clinical parameters are: End Diastolic Volume (EDV) = 139 mL, End Systolic Volume (ESV) = 53 mL, Stroke Volume = 86 mL, Ejection Fraction (EF) = 62%, and E/A = 1.5.

A controllable geometry of the MV is obtained from an ideal model through a mathematical description introduced in a previous study [17]. The radius of the valve, $R = 1.5$ cm, is kept constant (to adapt to the LV geometry) and with the normal elliptical shape (a parameter that describes the ratio between the length of the flaps in the two perpendicular directions set at a value of $1/3$). The asymmetry of this valve is described by a dimensionless parameter ϵ that mimics the difference in length between the anterior and the posterior leaflets, normalized to their sum [17]. The asymmetry is modified starting from an extreme value $\epsilon = 0.6$ to the opposite extreme $\epsilon = -0.6$, where the lengths of the anterior and posterior leaflet are $(1 + \epsilon)R$ and $(1 - \epsilon)R$, respectively. The analysis varies with continuity, with 25 positions selected with increments $\Delta\epsilon = 0.05$ between the two extreme values. In Figure 1, we show the complete geometry (a) with the semi-open valve at an instant indicated in the volume rate curve (b) and two MVs with asymmetry configurations, which are $\epsilon = 0.6$ and $\epsilon = -0.6$ (c,d). The MV geometries are reorganized for convenience in terms of another pair of parametric coordinates (ϑ, s), where s ranges from zero at the annulus to 1 and the trailing edge ϑ is the azimuthal angle.

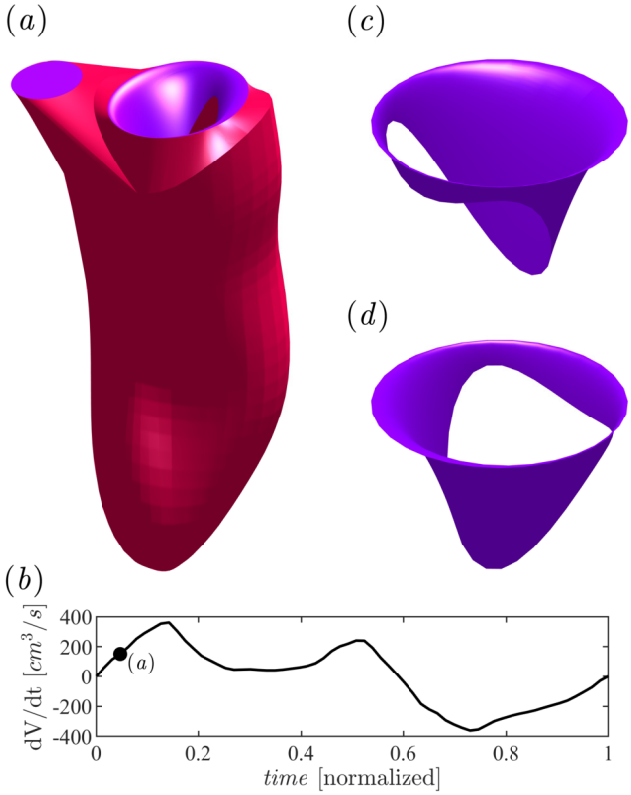

Figure 1. LV geometry (**a**) and its dV/dt curve (**b**). Ideal MV in semi-open configuration for $\epsilon = 0.6$ (**c**) and $\epsilon = -0.6$ (**d**), respectively.

The intermediate geometric configurations are reconstructed considering the two leaflets as moving independently of each other and each one associated with a degree of opening, say $\varphi_1(t)$ and $\varphi_2(t)$, for the anterior and posterior leaflets, respectively, that range from zero (closed leaflet) to $\frac{\pi}{2}$ (fully open). Therefore, the valve is mathematically described by its coordinates $\mathbf{X}_v(\vartheta, s, \varphi_1, \varphi_2)$. This parametric expression represents a two-dimensional set of all the possible valve configurations that are preliminarily calculated depending on two degrees of freedom (the opening degree of the two leaflets) between a fully closed configuration, $\mathbf{X}_v(\vartheta, s, 0, 0)$, when both angles are 0 and a fully open $\mathbf{X}_v(\vartheta, s, \frac{\pi}{2}, \frac{\pi}{2})$ when both angles are $\frac{\pi}{2}$. The dynamic equation of the leaflet-opening angles was obtained by the constraint that the motion of the leaflet surface must match the velocity of the fluid at the position of the same surface; a brief description is given below. A comprehensive description and verification of the computational method, including a comparison with a fluid–structure interaction model with a given set of tissue parameters, are reported elsewhere [15]. In synthesis, the valvular leaflets are assumed to move with the flow with no elastic resistance other than the constraint of remaining in the set of configurations described by the two degrees of freedom. Under this assumption, the leaflet dynamics are obtained by least-squares minimization of the difference, integrated over the valvular surface $\mathbf{A}_v$, between the fluid and the valve velocity component normal to the valvular surface. The result is a system of linear equations whose i^{th} term reads

$$\left[\int_{A_v}\left(\frac{\partial \mathbf{X}_v}{\partial \varphi_i}\cdot \boldsymbol{n}\right)\left(\frac{\partial \mathbf{X}_v}{\partial \varphi_j}\cdot \boldsymbol{n}\right)dA\right]\frac{d\varphi_j}{dt} = \int_{A_v}(\boldsymbol{v}\cdot \boldsymbol{n})\left(\frac{\partial \mathbf{X}_v}{\partial \varphi_i}\cdot \boldsymbol{n}\right)dA \quad (1)$$

where v is the fluid velocity and $\boldsymbol{n}$ the local normal to valvular surface. $i = 1, 2$, for the 2 degrees of freedom MV, and summation over $j = 1, 2$ is implicitly assumed. The dynamic

model described by system (1) represents an asymptotic limit of the loosest MV within the prescribed two-dimensional set of geometric configurations; as the model reproduces an asymptotic behavior, it does not require the introduction of mechanical parameters of the tissues that would otherwise be necessary for solving the momentum equation for the solid. On one hand, this is an advantage for applications where such properties are not available or cannot be measured; on the other, this model represents an approximation with respect to a complete calculation with fluid–structure interaction. This simplifies the solution that is aimed to reproduce the main properties of the LV fluid dynamics in the presence of a moving MV, assumed to have loose moving elements when the general properties of the valvular structure are not available. The absence of papillary muscles and chordae tendineae represent a limitation of the model. Here, the unidirectional valvular flow, avoiding the valve from opening towards the atrium, is ensured internally by the constraint on the degree of freedom that plays a surrogate function for the chordae tendinae. On the other hand, the presence of these anatomical structures inside the ventricle may influence the flow; however, the direct influence of these thin elements is expected to be marginal, and it was not evidenced in detailed analyses of blood flow recorded "in vivo" [18,19]. In this regard, this study has been extensively validated with an FSI model [15,16] and subsequently with a previous study [10] showing the homogeneity of the ideal MV with the real one and its movement. In the study by [20], it is shown how the presence of the chordae tendineae is not influential in the numerical simulation; the models with and without the cords showed similar results, and the essential thing is that the movement is faithfully reproduced, which was amply demonstrated for our cases [10,15,21–26]. A systematic analysis of the properties and limitations of such valvular modeling for flow simulation is reported in a dedicated methodological study [15]. The aortic valve, which is downstream of the LV flow fields, is modeled as a simple orifice with a surface that is either open or closed. This simple orifice model is represented by a surface that opens when two conditions apply: the MV is closed and the average normal velocity at the valve position is directed toward the aorta, and it is closed otherwise. In this way, it is not necessary to prescribe the open or closed state of the valve from global considerations because the exact start-to-end times of systole and diastole can be difficult to precisely define under pathological conditions. This AV model includes an explicit influence of the MV on the AV dynamics; on the other hand, the MV dynamics depends directly on the flow and by the fact that the AV is open or closed.

2.2. Fluid Dynamics

The numerical method is extensively described and validated in a dedicated methodological study [15], where the valvular dynamics are compared with those obtained by complete fluid–structure interaction [16]. In this section, we briefly recall the main points of the method used. The intraventricular fluid dynamics is evaluated by numerical solution of the Navier–Stokes and continuity equations

$$\frac{\partial \boldsymbol{v}}{\partial t} + \boldsymbol{v} \cdot \nabla \boldsymbol{v} = -\nabla p + \nu \nabla^2 \boldsymbol{v}, \tag{2}$$

$$\nabla \cdot \boldsymbol{v} = 0; \tag{3}$$

where $\boldsymbol{v}(t, \mathbf{x})$ is the velocity vector field, $p(t, \mathbf{x})$ is the kinematic pressure field and ν is the kinematic viscosity (assumed 0.04 cm^2/s). The solution is achieved by the immersed boundary method in a bi-periodic Cartesian domain as described in previous studies, e.g., [10,15,21,24,27]. Time advancement is achieved using a fractional step method as follows. Velocity is preliminarily advanced in time by the Navier–Stokes Equation (2) using a low-storage, third-order Runge–Kutta explicit scheme. Boundary conditions are set on the moving immersed boundaries that comprise the ventricle geometry and valve surface inside a bi-periodic domain with a grid made $128 \times 128 \times 160$ points and 8192 time steps per heartbeat. Then, the velocity is corrected by an irrotational field that projects the preliminary solution on a divergence-free vector field space.

2.3. Kinetic Energy and Dissipation Rate

The kinetic energy (KE) of the blood reflects a fundamental component of the work performed by the LV [28,29], and it is computed as follows

$$KE(t) = \frac{\rho}{2} \int_V v^2 \, dV, \tag{4}$$

where $V(t)$ is the ventricular volume, v the modulus of the velocity, and ρ the blood density. The KE dissipation rate

$$D(t) = \rho\nu \int_V S_{ij} \frac{\partial v_i}{\partial x_j} \, dV, \tag{5}$$

where S is the rate of deformation tensor and ν is the kinematic viscosity, provides a measure of the efficiency of blood flow and it is an indicator of ventricular function [25,30].

2.4. Vorticity and Vortex Formation Time

The formation of the vortex and its orientation inside the ventricle influence the correct course of the flow throughout the cardiac cycle until its expulsion [27,31]. The computation of the average vorticity inside the ventricle is

$$\overline{\omega} = \frac{1}{V} \int_V |\boldsymbol{\omega}| \, dV, \tag{6}$$

where $\boldsymbol{\omega}(t) = \nabla \times \boldsymbol{v}$ is the vorticity vector field. The vortex formation time (VFT) is an important parameter used for the evaluation of LV function [32]; this dimensionless parameter is computed as

$$VFT = \int_{T_E} D^{-1} \, v_{MVO} \, dt, \tag{7}$$

where v_{MVO} is the mean velocity across the MV orifice [10,21], D the average diameter, and T_E is the diastolic E-wave period. This parameter measures the quality of the vortex formation process and optimal LV filling. Recent studies [33] have shown that the optimal range is $3 \leq \text{VFT} \leq 4$, although a value up to 5 is also considered acceptable [34]. High values are associated with the breakdown of the forming vortex and turbulence, while lower values correspond to suboptimal propulsion [35].

2.5. Hemodynamic Forces

The forces exchanged between blood and the surrounding tissues have special relevance in ventricular function as they are found to have a role in modulating the response to morphogenesis in embryonic hearts [36], as well as to pathologies in adult hearts [37]. In particular, the hemodynamic force (HDF) is the global force exchanged that is made by the integral of the intraventricular pressure gradient and to a minor extent, of the viscous forces. HDF depends on the intraventricular flow and may help reveal a sub-optimal cardiac function when contraction or relaxation does not develop in association with a proper intraventricular pressure gradient. The HDF vector is obtained by the integral over the volume of the force density that is on the right side of (2) and can be computed by

$$\mathbf{F}(t) = \rho \int_{V(t)} \left[\frac{\partial \boldsymbol{v}}{\partial t} + \boldsymbol{v} \cdot \nabla \boldsymbol{v} \right] dV. \tag{8}$$

The volume integral in Equation (8) can also be rewritten, with the aid of the Gauss theorem, as a surface integral and evaluated from the dynamics of the endocardial boundary and the exchange of momentum across the mitral and aortic orifices [38]. This gives a formula equivalent to (8) that reads

$$\mathbf{F}(t) = \rho \int_{S(t)} \left[\boldsymbol{x} \left(\frac{\partial v}{\partial t} \cdot \boldsymbol{n} \right) + v(\boldsymbol{v} \cdot \boldsymbol{n}) \right] dS, \tag{9}$$

where $S(t)$ is the closed surface bounding the volume, comprising both the tissue and the valvular orifices, and $\boldsymbol{n}$ is the outward unit normal vector. The second expression (8) is often simpler to compute numerically and is used here.

3. Results

Fluid Dynamics, Vortex Formation, and Energetic Analysis

Before discussing the results, in Figure 2, we show the dV/dt curve obtained from the LV geometry superimposed to the diastolic flow rate measured across the MV in the two limit cases: LV with MV ($\epsilon = 0.6$ and $\epsilon = -0.6$, respectively). The three curves are not distinguishable as they overlap almost exactly; this preliminary validation test is aimed to confirm the consistency of the numerical results and the equality of the amount of blood entering for all cases to verify that any variation is imputable to the MV asymmetry only.

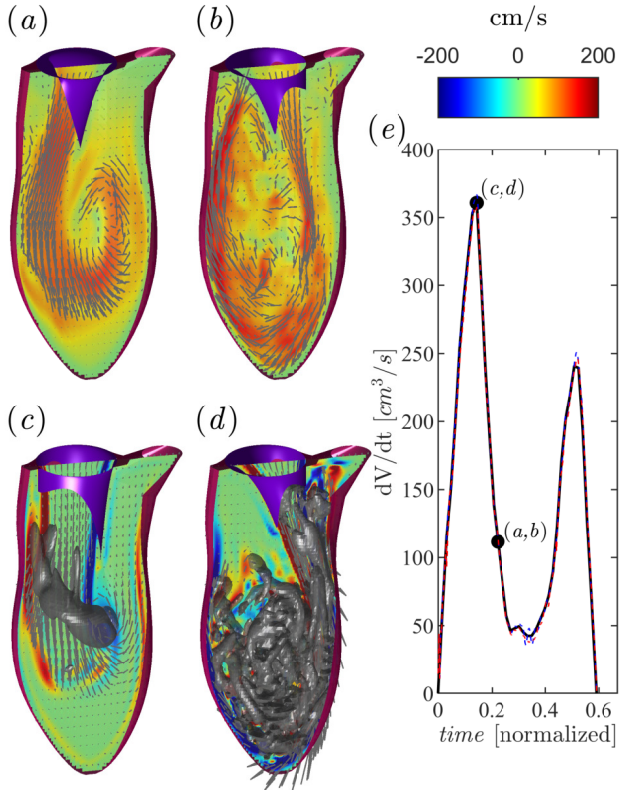

Figure 2. Velocity field of MV with (**a**) $\epsilon = 0.6$, (**b**) $\epsilon = -0.6$; flow field of MV with (**c**) $\epsilon = 0.6$, (**d**) $\epsilon = -0.6$ as indicated in the box of the dV/dt curve (**e**); the normal vorticity is shown in red to blue color from -200 units to 200 units (cm/s) equal to the inverse of the heartbeat period and the velocity vector (every 4 grid points) on a longitudinal plane crossing the center of MV of the aorta and the LV apex; the three-dimensional gray surfaces represent one isosurface of the λ_2 parameter.

In Figure 2a,b, we show the directionality of the diastolic flow inside the ventricle in the two limit cases ($\epsilon = 0.6$ and $\epsilon = -0.6$), and a more complete view of the intermediate points is shown in a previous study [10]. As seen in the previously mentioned study, a valve with positive asymmetry directs the flow to a physiological rotation with its extreme shape shown in Figure 2a; in the case of negative asymmetry, the direction of the flow is reversed and increases its velocity, which maintains the reversed flow direction during the entire filling phase. A very positive asymmetry highlights the predominance of the posterior leaflet with a very deviating flow toward the posterior wall; as we approach a more balanced direction between the two leaflets, the flow takes a more regular and physiological direction, while negative asymmetry reverses the flow direction and makes the valve behave as if it were reversed. This demonstrates qualitatively how the leaflet's asymmetry affects the direction of the flow. In Figure 2c we show the formation and direction of the vortex

ring in case with ϵ = 0.6. Compared with an ideal healthy case [10,15], the vortex is inclined and directed towards the left wall of the LV similarly to various pathological valve cases [10,21,23]. Instead, in Figure 2d, the flow is inverted ($\epsilon = -0.6$), the vortex breaks very early, and the vorticity increases due to the generation of turbulence inside the LV.

This point is supported by the result shown in Figure 3a reporting the $\overline{\omega}_{E_{peak}}$ values that are higher for $\epsilon-$ and decrease as the curve transits towards $\epsilon+$. This is also confirmed by the VFT values in Figure 3b. These results indicate how effectively an MV with $\epsilon-$ actually affects the ability of the LV to redirect flow to the systolic outlet. In fact, the VFT reaches more physical values when it approaches the direction of positive asymmetry, showing how good ventricular functionality corresponds to the correct distribution of the flow. Taking into account the values published in a previous work [22] and the existing literature [32–35], we identify an optimal range between ϵ = 0.15 and 0.6, considering that after ϵ = 0.4, fairly stationary values are found.

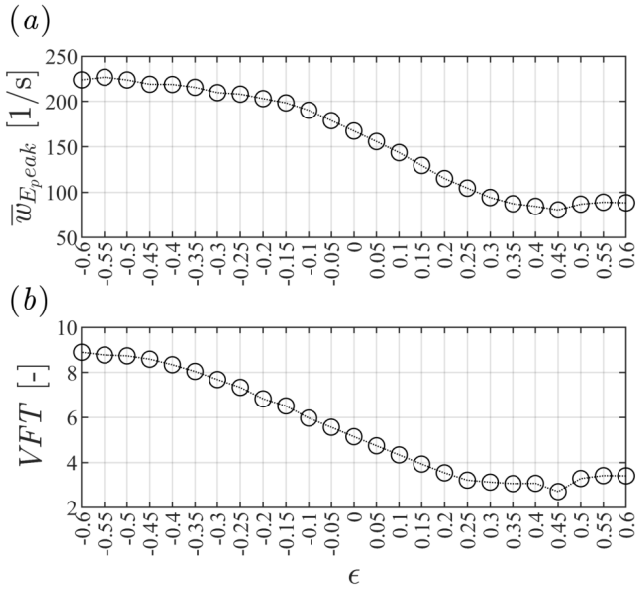

Figure 3. Graphical representation of (**a**) diastolic peak values of mean vorticity and (**b**) VFT values for different valve asymmetry.

The same behavior is found in terms of $KE_{E_{peak}}$, as shown in Figure 4a. The $KE_{E_{peak}}$ is higher for $\epsilon = -0.6$ and the distribution of these values for each level of valve asymmetry follows the same trend as in Figure 3. This production of KE is due to the higher mitral jet velocity in line with the orientation of the flow and the vorticity produced. When the valve asymmetry is reduced, the quantity of $KE_{E_{peak}}$ decreases until it returns to a more physiological value. Furthermore, in this case, there is an evident transition between positive and negative asymmetry. From the literature, it is easy to identify a normal range from the experimental observation performed with 4D Flow MR; this value is between 6 ± 0.6 for control cases [28] and 8.9 ± 1.1 for athletes [39]. The energy dissipation rate, $D_{E_{peak}}$, also follows the same trend and is in line with the existing values [22,40]; eventually from these results, the optimal values for valve asymmetry appear above ϵ = 0.2.

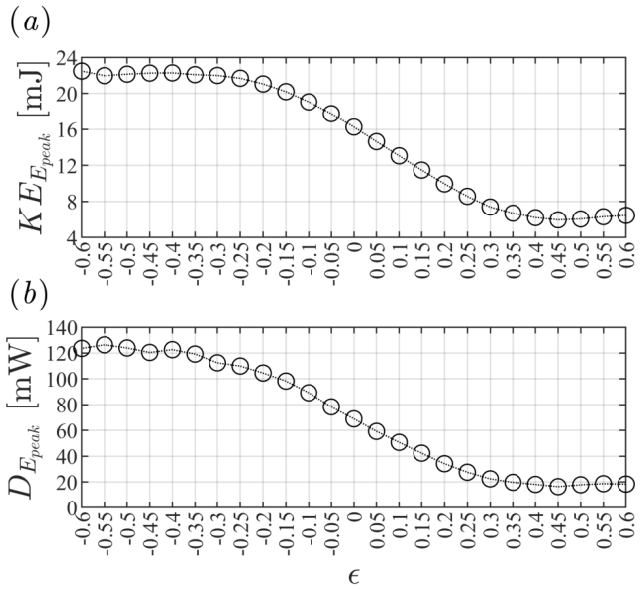

Figure 4. Graphical representation of (**a**) diastolic peak values of KE and (**b**) D for different valve asymmetry.

Figure 5a–c report the three components of the hemodynamic force during the E-wave curve. In panel (a), it can be seen how the sign of the x-component, Fx, where the x-axis is the lateral direction along the ideal line connecting the two valves, is largely affected by the asymmetry level until changing its sign. This is due to the different lengths and positions that the leaflets assume in different asymmetrical conditions. To confirm this, there is literature that describes the E-wave of the HDFs in the direction of x as positive [37,38,41–43], thus again marking the choice of $\epsilon-$ in a valve repair or design as non-physiologic. In the transverse direction, Fy values are similar and do not vary much; this is desirable since this direction is not directly affected by the valve movement. In the longitudinal direction, on the other hand, an increase in Fz can be noted in the $\epsilon-$ cases. This increase is not very high from the point of view of normality [44], but it may become relevant when it is a result of a valve repair or replacement. The $\epsilon+$ values are in line with the literature for healthy cases, while the $\epsilon-$ values are in line with the literature for healthy athletes and therefore require a trained heart [41,43]. A patient who undergoes cardiac surgery usually has a heart with very variable EF and dysfunctions dictated by valvular pathology. Repairing or replacing an MV with a non-physiological degree of valve asymmetry could induce higher stress to the ventricular tissues. This is important because the presence of the physiological components HDF support the correct redirection of blood from the MV towards the LV outflow tract, which does not occur in $\epsilon-$ cases. These results are summarized in Figure 5d–f, where the absolute values at peak systole are reported for different valve asymmetry. values This figure is useful for identifying the range and the optimal asymmetry value. In $|Fx_{E_{peak}}|$, there is a minimum point at $\epsilon = 0.3$, which corresponds to the asymmetry level that produces no lateral thrust, therefore, where the intraventricular pressure gradient is directed—on average—from the base to the apex. The transversal force $|Fy_{E_{peak}}|$ presents a variation in values that is minimal, irrelevant, and fairly constant for all $\epsilon+$ cases, while the longitudinal force, $|Fz_{E_{peak}}|$, displays a rapid decrease up to $\epsilon = 0.3$ and then moves into a stationary phase.

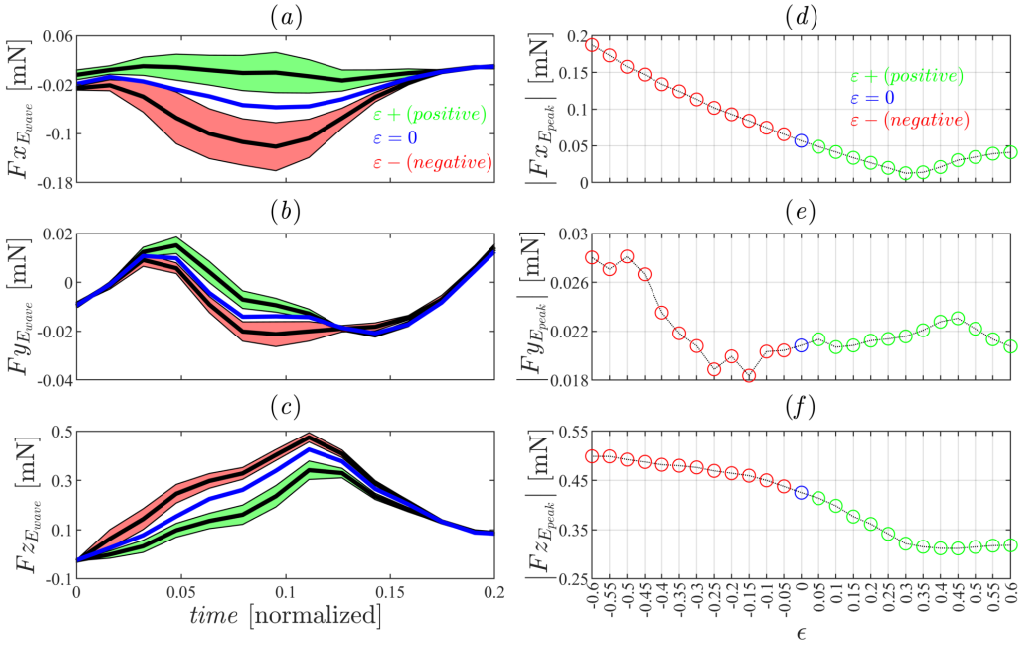

Figure 5. Graphical representation of HDF E-wave curve for different valve asymmetry of (**a**) Fx, (**b**) Fy and (**c**) Fz projections. Green color represent the SD of $\epsilon+$, blue line $\epsilon = 0$, red color the SD of $\epsilon-$ and black line the mean value for $\epsilon+$ and $\epsilon-$, respectively. Graphical representation of the HDF peak for different valve asymmetries of (**d**) $|Fx|$, (**e**) $|Fx|$ and (**f**) $|Fx|$ projections. Green represents $\epsilon+$, blue represents $\epsilon = 0$, and red represents $\epsilon-$.

4. Conclusions

The evaluation and determination of the proper valve asymmetry are crucial in cardiac surgery because a correct repair or a correct valve implant substantially increases the possibility of a long and better quality of life [45,46]. In a previous study on valve asymmetry [10], it was shown that an MV with negative asymmetry behaves like a turned MV. Those results show how the different asymmetrical positions of the leaflets and their length influence the flow direction inside the LV, affecting the amount of blood regurgitated in the atrium during systole in healthy, pathological, and repaired MV conditions. The ideal range is identified therein between ϵ = 0.2 and ϵ = 0.4 based on a global assessment of the ventricular washout. With this study, we extend the analysis including energetic and dynamic assessments using a different healthy LV. After verifying and confirming that the ventricular flow trend is equal to the previous study, we also verified the vortex formation and the vorticity generated in different situations of valve asymmetry. The results show how an $\epsilon-$ produces inverted flow and a vortex breaking early, generating high vorticity, which, associated with VFT, indicates the ventricular difficulty of directing the flow towards the systole, such that the ventricle is more stressed and fatigued. Consequently, high and non-physiological values of KE and D also confirm this and decrease with the reduction in ϵ until more natural values of $\epsilon+$ are obtained. The HDFs further highlighted this gap between $\epsilon-$ and $\epsilon+$ in an evident way in the Fx component, where the length and position of the two leaflets influence the orientation of the diastolic curve, making it non-physiological for $\epsilon-$ and positive for $\epsilon+$. In a more detailed way, the Fz component shows that the negative asymmetry values produce values similar to each other and comparable to an athlete's heart that does not find comfort, as occurs in patients who undergo these surgical practices in non-optimal conditions even with a preserved EF. The diastolic function of the LV plays an important role in cardiac physiology. Lusitropia, the ability of cardiac myocytes to relax, is affected by both biochemical events within the myocyte and biomechanical events in the LV [47]. An abnormal diastolic function has been recognized in many cardiovascular diseases and is associated with worse outcomes, including total mortality and hospitalizations for heart failure [48]. These results show

how $\epsilon-$ negatively influences diastolic function, indicating that MV repair or replacement in this direction has to be avoided. The optimal range of ϵ is between 0.2 and 0.4 with an optimum point of about 0.3. Despite the modeling limitations of the analysis, optimal values of asymmetry agree well with physiological values of asymmetry, as visible from the length of MV leaflets in healthy subjects [49]. The computational model used here should not be confused with an FSI model, primarily because it does include the elastic properties of the tissues that would be required to solve the momentum equation for the solid elements. Therefore, it describes an asymptotic behavior only and was designed to provide a relatively straightforward application of LV flow simulations in clinical conditions when the mechanical properties of tissue are not available or cannot be extrapolated. To reach this objective, the model includes a number of simplifications that correspond to a series of limitations that are described in a previous methodological article [15]. However, this model is already used and validated in the clinical setting for the evaluation of various physiological and pathological conditions [10,15,21–23,50]. Our results provide an indication before surgery, which can make it clearer to surgeons which type of valve asymmetry to use for a correct valve repair/replacement and above all what to expect in the case of a different solution. This could be a great help in preventing disastrous consequences and in directing the patient towards an optimal clinical condition. A limitation of this study is the lack of extension to cases with pathological LV; this is a deliberate choice to make a first complete valvular analysis. This evaluation will be extended to several LV cases in a subsequent study.

Author Contributions: D.C. and G.P. have made a substantial, direct and intellectual contribution to the work. All authors have read and agreed to the published version of the manuscript.

Funding: This research was funded by the Italian Ministry of Education, Universities and Research (MIUR); MIUR code: 2017A889FP_ 006; CUP code: J34I19001480001.

Institutional Review Board Statement: Not applicable.

Informed Consent Statement: The images of the human subjects were recorded at the Cardiovascular Department of the Azienda Sanitaria Universitaria Giuliano Isontina, Trieste. The geometries were provided in an anonymous form for the numerical study. All procedures involving human subjects have been performed in accordance with the Declaration of Helsinki and under the approval of the Ethics Committee of the University of Trieste (protocol no. 0025052).

Data Availability Statement: All data generated or analysed during this study are included in this published article.

Acknowledgments: The authors acknowledge the Research Project of National Interest PRIN 2017 "Fluid dynamics of hearts at risk of failure: towards methods for the prediction of disease progression".

Conflicts of Interest: The authors declare no conflict of interest.

References

1. Freed, A.; Levy, D.; Levine, R.A.; Larson, M.G.; Evans, J.C.; Fuller, D.L.; Lehman, B.; Benjamin, E.J. Prevalence and clinical outcome of mitral-valve prolapse. *N. Engl. J. Med.* **1999**, *341*, 1–7. [CrossRef]
2. Shapira, Y.; Vaturi, M.; Sagie, A. Hemolysis associated with prosthetic heart valves: A review. *Cardiol. Rev.* **2009**, *17*, 121–124. [CrossRef] [PubMed]
3. Cooper, K.C.; Wagner, R. Xenotransplantation. *Nonhum. Primates Biomed. Res.* **2012**, *1*, 391–402.
4. Adams, D.H.; Rosenhek, R.; Falk, V. Degenerative mitral valve regurgitation: Best practice revolution. *Eur. Heart J.* **2010**, *31*, 1958–1966. [CrossRef] [PubMed]
5. Elbey, M.A.; Dalan, L.P.; Attizzani, G.F. Value of MitraClip in reducing functional mitral regurgitation. *US Cardiol. Rev.* **2019**, *13*, 30. [CrossRef]
6. Castillo, J.G.; Anyanwu, A.C.; Fuster, V.; Adams, D.H. A near 100% repair rate for mitral valve prolapse is achievable in a reference center: Implications for future guidelines. *J. Thorac. Cardiovasc. Surg.* **2012**, *144*, 308–312. [CrossRef]
7. Carpentier, A. Cardiac valve surgery-the 'French correction'. *J. Thorac. Cardiovasc. Surg.* **1983**, *86*, 323–337. [CrossRef]
8. Colli, A.; Adams, D.H.; Fiocco, A.; Pradegan, N.; Longinotti, L.; Nadali, M.; Pandis, D.; Gerosa, G. Transapical NeoChord mitral valve repair. *Ann. Cardiothorac. Surg.* **2018**, *7*, 812–320. [CrossRef]

9. Stone, G.W.; Lindenfeld, J.A.; Abraham, W.T.; Kar, S.; Lim, D.S.; Mishell, J.M.; Whisenant, B.; Grayburn, P.A.; Rinaldi, M.; Kapadia, S.R.; et al. Transcatheter mitral-valve repair in patients with heart failure. *N. Engl. J. Med.* **2018**, *379*, 2307–2318. [CrossRef]
10. Collia, D. Mitral valve asymmetry in healthy, pathological, and repaired cases. *Phys. Fluids* **2021**, *22*, 077118. [CrossRef]
11. Danilov, A.; Lozovskiy, A.; Olshanskii, M.; Borgquist, R.; Vassilevski, Y. A finite element method for the Navier–Stokes equations in moving domain with application to hemodynamics of the left ventricle. *Russ. J. Numer. Anal. Math. Model.* **2017**, *32*, 225–236. [CrossRef]
12. Peskin, C.S. Numerical Analysis of Blood Flow in the Heart. *J. Comput. Phys.* **1977**, *25*, 220–252. [CrossRef]
13. Zakerzadeh, R.; Hsu, M.C.; Sacks, M.S. Computational methods for the aortic heart valve and its replacements. *Expert Rev. Med. Devices* **2017**, *14*, 849–866. [CrossRef] [PubMed]
14. Vassilevski, Y.; Liogky, A.; Salamatova, V. Application of Hyperelastic Nodal Force Method to Evaluation of Aortic Valve Cusps Coaptation: Thin Shell vs. Membrane Formulations. *Mathematics* **2021**, *9*, 1450. [CrossRef]
15. Collia, D.; Vukicevic, M.; Meschini, V.; Zovatto, L.; Pedrizzetti, G. Simplified mitral valve modeling for prospective clinical application of left ventricular fluid dynamics. *J. Comput. Phys.* **2019**, *398*, 108895. [CrossRef]
16. Meschini, V.; de Tullio, M.; Querzoli, G.; Verzicco, R. Flow structure in healthy and pathological left ventricles with natural and prosthetic mitral valves. *J. Fluid Mech.* **2018**, *834*, 271–307. [CrossRef]
17. Domenichini, F.; Pedrizzetti, G. Asymptotic Model of Fluid—Tissue Interaction for Mitral Valve Dynamics. *Cardiovasc. Eng. Technol.* **2015**, *6*, 95–104. [CrossRef]
18. Elbaz, M.S.M.; Calkoen, E.E.; Westenberg, J.J.M.; Lelieveldt, B.P.F.; Roest, A.A.W.; van der Geest, R.J. Vortex flow during early and late left ventricular filling in normal subjects: Quantitative characterization using retrospectively-gated 4D flow cardiovascular magnetic resonance and three-dimensional vortex core analysis. *J. Cardiovasc. Magn. Reson.* **2014**, *16*, 78. [CrossRef]
19. Arvidsson, P.M.; Kovács, S.J.; Töger, J.; Borgquist, R.; Heiberg, E.; Carlsson, M.; Arheden, H. Vortex ring behavior provides the epigenetic blueprint for the human heart. *Sci. Rep.* **2016**, *6*, 22021. [CrossRef]
20. Meschini, V.; de Tullio, M.D.; Verzicco, R. Effects of mitral chordae tendineae on the flow in the left heart ventricle. *Eur. Phys. J. E* **2018**, *41*, 27. [CrossRef]
21. Collia, D.; Zovatto, L.; Pedrizzetti, G. Analysis of mitral valve regurgitation by computational fluid dynamics. *APL Bioeng.* **2019**, *3*, 036105. [CrossRef] [PubMed]
22. Collia, D.; Zovatto, L.; Tonti, G.; Pedrizzetti, G. Comparative Analysis of Right Ventricle Fluid Dynamics. *Front. Bioeng. Biotech.* **2021**, *9*, 667408. [CrossRef] [PubMed]
23. Collia, D.; Pedrizzetti, G. Cardiac Fluid Dynamics in Prolapsed and Repaired Mitral Valve. In Proceedings of the XXIV AIMETA Conference 2019, Rome, Italy, 15–19 September 2019; Carcaterra, A., Paolone, A., Graziani, G., Eds.; Lecture Notes in Mechanical Engineering; Springer: Cham, Switzerland, 2020; pp. 857–867.
24. Pedrizzetti, G.; Canna, G.L.; Alfieri, O.; Tonti, G. The vortex an early predictor of cardiovascular outcome? *Nat. Rev. Cardiol.* **2008**, *11*, 545–553. [CrossRef] [PubMed]
25. Pedrizzetti, G.; Domenichini, F. Left ventricular fluid mechanics: The long way from theoretical models to clinical applications. *Ann. Biomed. Eng.* **2015**, *43*, 26–40. [CrossRef]
26. Celotto, C.; Zovatto, L.; Collia, D.; Pedrizzetti, G. Influence of mitral valve elasticity on flow development in the left ventricle. *J. Biomech.* **2019**, *75*, 110–118. [CrossRef]
27. Domenichini, F. On the consistency of the direct forcing method in the fractional step solution of the navier–stokes equations. *J. Comput. Phys.* **2008**, *227*, 6372–6384. [CrossRef]
28. Carlsson, M.; Heiberg, E.; Toger, J.; Arheden, H. Quantification of left and right ventricular kinetic energy using four-dimensional intracardiac magnetic resonance imaging flow measurement. *J. Heart Circ. Physiol.* **2011**, *302*, 893–900. [CrossRef]
29. Garg, P.; Crandon, S.; Swoboda, P.P.; Fent, G.J.; Foley, J.R.J.; Chew, P.G.; Brown, L.A.E.; Vijayan, S.; Hassell, M.E.C.J.; Nijveldt, R.; et al. Left ventricular blood flow kinetic energy after myocardial infarction—Insights from 4d flow cardiovascular magnetic resonance. *J. Cardiovasc. Magn. Res.* **2018**, *20*, 2344–2350. [CrossRef]
30. Hayashi, T.; Itatani, K.; Inuzuka, R.; Shimizu, N.; Shindo, T.; Hirata, Y.; Miyaji, K. Dissipative energy loss within the left ventricle detected by vector flow mapping in children: Normal values and effects of age and heart rate. *J. Cardiol.* **2015**, *66*, 403–410. [CrossRef]
31. Kilner, P.; Yang, G.; Wilkes, A.J.; Mohiaddin, R.; Firmin, D.; Yacoub, M. Asymmetric redirection of flow through the heart. *Nature* **2000**, *404*, 759–761. [CrossRef]
32. Kheradvar, A.; Rickers, C.; Morisawa, D.; Kim, M.; Hong, G.; Pedrizzetti, G. Diagnostic and prognostic significance of cardiovascular vortex formation. *J. Cardiol.* **2019**, *74*, 403–411. [CrossRef] [PubMed]
33. King, G.; Ngiam, N.; Clarke, J.; Wood, M.J.; Poh, K.K. Left ventricular vortex formation time in elite athletes. *Int. J. Cardiovasc. Imaging* **2019**, *35*, 307–311. [CrossRef]
34. Kheradvar, A.; Assadi, R.; Falahatpisheh, A.; Sengupta, P.P. Assessment of Transmitral Vortex Formation in Patients with Diastolic Dysfunction. *JASE* **2012**, *25*, 220–227. [CrossRef] [PubMed]
35. Mangual, J.O.; Kraigher-Krainer, E.; De Luca, A.; Toncelli, L.; Shah, A.; Solomon, S.; Galantic, G.; Domenichini, F.; Pedrizzetti, G. Comparative numerical study on left ventricular fluid dynamics after dilated cardiomyopathy. *J. Biomech.* **2013**, *46*, 1611–1617. [CrossRef] [PubMed]

36. Hove, J.R.; Köster, R.W.; Forouhar, A.S.; Acevedo-Bolton, G.; Fraser, S.E.; Gharib, M. Intracardiac fluid forces are an essential epigenetic factor for embryonic cardiogenesis. *Nature* **2003**, *421*, 172–177. [CrossRef]
37. Arvidsson, P.M.; Töger, J.; Carlsson, M.; Steding-Ehrenborg, K.; Pedrizzetti, G.; Heiberg, E.; Arheden, H. Left and right ventricular hemodynamic forces in healthy volunteers and elite athletes assessed with 4D flow magnetic resonance imaging. *Am. J. Physiol. Heart Circ. Physiol.* **2017**, *312*, H314–H328. [CrossRef]
38. Pedrizzetti, G. On the computation of hemodynamic forces in the heart chambers. *Am. J. Physiol. Heart Circ. Physiol.* **2019**, *95*, 109323. [CrossRef]
39. Steding-Ehrenborg, K.; Arvidsson, P.; Töger, J.; Rydberg, M.; Heiberg, E.; Carlsson, M. Determinants of kinetic energy of blood flow in the four-chambered heart in athletes and sedentary controls. *Am. J. Physiol. Heart Circ. Physiol.* **2016**, *310*, 113–122. [CrossRef]
40. Seo, J.; Mittal, R. Effect of diastolic flow patterns on the function of the left ventricle. *Phys. Fluids* **2013**, *25*, 110801. [CrossRef]
41. Pedrizzetti, G.; Arvidsson, M.; Töger, J.; Borgquist, R.; Domenichini, F.; Arheden, H.; Heiberg, E. On estimating intraventricular hemodynamic forces from endocardial dynamics: A comparative study with 4D flow MRI. *J. Biomech.* **2017**, *60*, 203–210. [CrossRef]
42. Arvidsson, P.M.; Töger, G.; Pedrizzetti, G.; Heiberg, E.; Borgquist, R.; Carlsson, M.; Arheden, H. Hemodynamic forces using four-dimensional flow MRI: an independent biomarker of cardiac function in heart failure with left ventricular dyssynchrony? *Am. J. Physiol. Heart Circ. Physiol.* **2018**, *315*, H1627–H1639. [CrossRef]
43. Vallelonga, F.; Airale, L.; Tonti, G.; Argulian, E.; Milan, A.; Narula, J.; Pedrizzetti, G. Introduction to Hemodynamic Forces Analysis: Moving Into the New Frontier of Cardiac Deformation Analysis. *J. Am. Heart Assoc.* **2013**, *10*, e023417. [CrossRef]
44. Faganello, G.; Collia, D.; Furlotti, S.; Pagura, L.; Zaccari, M.; Pedrizzetti, G.; Di Lenarda, A. A new integrated approach to cardiac mechanics: reference values for normal left ventricle. *Int. J. Cardiovasc. Imaging* **2020**, *36*, 2173–2185. [CrossRef]
45. Schnittman, S.R.; Itagaki, S.; Toyoda, N.; Adams, D.H.; Egorova, N.N.; Chikwe, J. Survival and long-term outcomes after mitral valve replacement in patients aged 18 to 50 years. *J. Thorac. Cardiovasc. Surg.* **2018**, *155*, 96–102. [CrossRef]
46. Chikwe, J.; Toyoda, N.; Anyanwu, A.C.; Itagaki, S.; Egorova, N.N.; Boateng, P.; El-Eshmawi, A.; Adams, D.H. Relation of Mitral Valve Surgery Volume to Repair Rate, Durability, and Survival. *J. Am. Coll. Cardiol.* **2018**, *69*, 2397–2406. [CrossRef]
47. Villars, P.S.; Hamlin, S.K.; Shaw, A.D.; Kanusky, J.T. Role of diastole in left ventricular function, I: Biochemical and biomechanical events. *Am. J. Crit. Care* **2004**, *13*, 394–403. [CrossRef]
48. Nagueh, S.F. Left Ventricular Diastolic Function: Understanding Pathophysiology, Diagnosis, and Prognosis with Echocardiography. *JACC Cardiovasc. Imaging* **2020**, *13*, 228–244. [CrossRef]
49. Oliveira, D.; Srinivasan, J.; Espino, D.; Buchan, K.; Dawson, D.; Shepherd, D. Geometric description for the anatomy of the mitral valve: A review. *J. Anat.* **2020**, *237*, 209–224. [CrossRef]
50. Pandis, D.; Anyanwu, A. Commentary: Four-dimensional left ventricular flow imaging after surgical valve reconstruction—Pretty pictures or marker of repair quality? *J. Thorac. Cardiovasc. Surg.* **2020**, *163*, 962–964. [CrossRef]